

Diffused metal-insulator transition in NdNiO₃ film grown on BaTiO₃: Likely evidence of electronic Griffiths phase

Parushottam Majhi,^{1,*} Sudipta Chatterjee,^{1,*} Ravindra Singh Bisht,¹ V. Raghavendra Reddy,²
Barnali Ghosh,¹ and A. K. Raychaudhuri^{3,†}

¹*Department of Condensed Matter Physics and Materials Science, S.N. Bose National Centre for Basic Sciences,
JD Block, Sector III Salt Lake, Kolkata 700106, India*

²*UGC-DAE Consortium for Scientific Research, University Campus, Khandwa Road, Indore 452001, India*

³*CSIR Centre for Glass and Ceramic Research Institute, 196 Raja S.C. Mullick Road, Kolkata 700032, India*



(Received 1 April 2021; accepted 22 July 2021; published 13 August 2021)

This paper reports diffused metal-insulator transitions (MITs) in an oxide with disorder that undergoes a Mott transition. The investigation was carried out in the multilayer film NdNiO₃/BaTiO₃/SrTiO₃ (NNO/BTO/STO), where a large mismatch of lattice constants of NNO with those of BTO leads to strain relaxation and creation of quenched disorder in the NNO film. NNO film in the NNO/BTO/STO multilayer structure shows a broad Mott-type MIT at a temperature $T_{\text{MI}} = 160$ K from a high-temperature bad metallic phase ($\frac{1}{\rho_{\text{DC}}} \frac{d\rho_{\text{DC}}}{dT} < 0$) with a high value of resistivity $\rho_{\text{DC}} \approx 70$ m Ω cm at 300 K to a low temperature insulating phase. Using noise spectroscopy and impedance spectroscopy which can probe the dynamics of the coexisting phases near the MIT, it was observed that in addition to the MIT at $T_{\text{MI}} = 160$ K, there exists a characteristic temperature $T_G \approx 230$ K well above the T_{MI} , where large low-frequency correlated fluctuations appear, signifying the appearance of a phase with slow dynamics. T_G signals the onset of a temperature region $T_{\text{MI}} < T < T_G$ with coexisting phases that have been corroborated by the impedance spectroscopy and AC conductivity measurements. It is suggested that the temperature T_G may signify the onset of an electronic Griffiths phase that has been theoretically proposed for Mott transitions with disorder.

DOI: [10.1103/PhysRevMaterials.5.085005](https://doi.org/10.1103/PhysRevMaterials.5.085005)

I. INTRODUCTION

Investigation of correlation-driven Mott-type metal insulator transition (MITs) in solids with disorder is a topic of considerable current interest [1–4]. In general, the first-order Mott transition in pristine samples without disorder occurs at a well-defined temperature T_{MI} where the low temperature insulating phase sets in on cooling. For $T > T_{\text{MI}}$, the stable phase is a metallic phase with considerably lower resistivity. The Mott transition, like any other first-order phase transition, is accompanied by hysteresis [5] although the width of the transition can be very small. Presence of disorder in first-order transition rounds off the transition and in some cases the first-order transition ends in a critical point. However, the presence of both disorder and correlation in samples undergoing MITs can make the transition diffused with a transition region that extends over a considerable temperature range with coexisting phases. The coexisting phases are the low-temperature high resistivity insulating phase and the high-temperature less resistive metallic phase. The present paper is an experimental investigation of MIT in a system with disorder undergoing a Mott transition of diffused nature. The paper explores whether in such a system one can observe the

likely appearance of electronic Griffiths phase as a precursor to the MIT.

Theoretical investigations of Mott-Anderson transitions with interactions and disorder concluded the occurrence of an electronic Griffiths phase [6–10] near the transition. It has been proposed that there is a universal occurrence of electronic Griffiths phase as a precursor of MIT in correlated electronic systems with disorder [10,11]. While the occurrence of an electronic Griffiths phase close to the Mott-type MIT is a well-developed theoretical concept, there are not too many reports of experiments that show evidence of existence of such a phase. Very recently, evidence of an electronic Griffiths phase had been seen in an organic Mott system with disorder where the conduction bandwidth had been controlled by hydrostatic pressure and disorder by x-ray irradiation. The signature of the Griffiths phase close to but above the T_{MI} manifested itself through the occurrence of slow kinetics of relaxation as measured by NMR relaxation [12]. While there are well-known correlated oxide systems such as NdNiO₃, VO₂, and V₂O₃ that show Mott-type transitions, occurrence of the electronic Griffiths phase in such correlated oxide systems has not been reported.

NdNiO₃ (NNO) films grown on different lattice-matched crystalline substrates have been studied extensively in recent years to investigate the correlation-driven MIT [13,14]. It has been established that in coherently strained epitaxial films of NNO, the built-in strain can tune T_{MI} . In a recent investigation by our group carried out on films of NNO on LaAlO₃

*These authors contributed equally to this work.

†arupraychaudhuri4217@gmail.com

(LAO), it was shown by using spatially resolved scanning tunneling spectroscopy that there are coexisting regions of a low-temperature insulating phase and a high-temperature metallic phase close to the transition region [15]. Coexisting electronic phases with a percolative nature can lead to interesting behavior in noise spectroscopy as well as in impedance spectroscopy (IS) if there is a dynamics associated with the phase co-existence. We investigate in this paper whether a large lattice mismatch of the film with the substrate can make the MIT diffuse due to quenched disorder. We also propose to explore whether this leads to the occurrence of a Griffiths phase [16]. Despite extensive work on MIT in NNO films (and also in other correlated oxide films), the existence of a temperature T_G , at which Griffiths phase sets in above the MIT has not been investigated.

The current investigation has been carried out on NNO film grown on BaTiO₃ (BTO) film with which the former has a substantial lattice mismatch. The BTO film, in turn, was grown on a crystalline SrTiO₃ (STO) (100) substrate. The multilayer sample is referred to as NNO/BTO/STO. Though the NNO films as well as BTO films so grown are oriented and highly textured, the large lattice mismatch and larger thickness of the films lead to strain relaxation in the films, leading to creation of quenched disorder and in-plane and out-of-plane residual strains as well as local strain inhomogeneity. The metallic state in such NNO films shows a bad metallic phase with high resistivity and a negative temperature coefficient of resistivity (TCR) ($\equiv \frac{1}{\rho} \frac{d\rho}{dT}$) < 0 . The observed MIT is thus from a bad metal to an insulator. This is unlike MIT seen in NNO films grown on lattice-matched substrates like STO or LAO or even good bulk pellets where the high-temperature metallic phase mostly have a resistivity $\sim 1\text{--}5$ m Ω cm and a positive TCR. We observe that the temperature-dependent ρ shows a percolative nature of transport occurring due to coexisting phases and the transition region is broad. We also find that in such a film there exists a temperature, which we refer as T_G ($> T_{MI}$), where there is an appearance of substantial correlated low-frequency fluctuation, slowing down of relaxation time of the correlated fluctuations, and evidence of anomalous behavior as observed from the IS. We explore whether T_G can be identified as the onset temperature of an electronic Griffiths phase in the temperature range $T_{MI} < T < T_G$. This is an electronic analog of the magnetic Griffiths temperature.

II. EXPERIMENTAL DETAILS

The NNO film (thickness ≈ 30 nm) used in this experiment was deposited on a film of BTO (thickness ≈ 120 nm) grown on STO single crystalline substrate with (100) orientation. The films were deposited sequentially without breaking vacuum by pulse laser deposition with KrF laser ($\lambda = 248$ nm) using well-characterized BTO and NNO pellets as targets. The films after growth were given one-hour annealing in one atmosphere of oxygen at 700 °C. Details of NNO film growth have been given in a previous publication [15].

The films were characterized by x-ray diffraction (XRD) and scanning probe microscopy. The x-ray reciprocal space mapping (RSM) was obtained in a Bruker D8-Discover system using Cu K α radiation. The Bruker D8 system is equipped with a Eulerian cradle, Goebel mirror, and LynxEye detector.

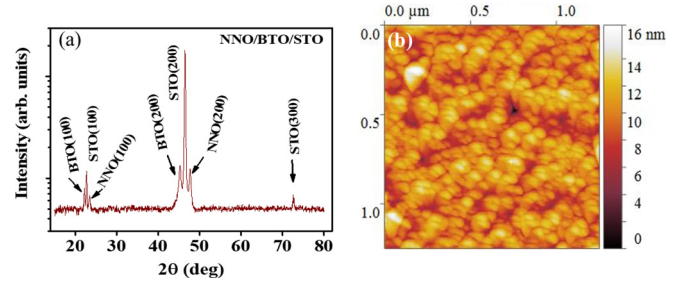


FIG. 1. (a) X-ray diffraction pattern of the NNO/BTO/STO multilayer film. (b) Scanning probe microscope image of $1.3 \mu\text{m} \times 1.3 \mu\text{m}$ area of the film.

The data were analyzed with LEPTOS software. Information on elastic constants needed for the analysis were obtained from published data [17].

The temperature-dependent DC resistivity ($\rho_{DC}(T)$) was measured in the temperature interval $4 \text{ K} < T < 300 \text{ K}$ using a four-probe collinear geometry with Cr/Au contact pads in a closed cycle cryostat. The temperature and frequency ($\omega = 2\pi f$) dependent IS measurements were done by measuring the real part Z' and the imaginary part Z'' of the complex impedance $Z = Z' + iZ''$ with a LCR meter in the frequency range $100 \text{ Hz} < f < 1 \text{ MHz}$ in a planar geometry with current in plane of the film. The temperature range of measurement for IS is down to 80 K. Open-circuit and short-circuit compensations were done to take care of the capacitive and inductive contributions of the connecting coaxial cables.

The noise measurements (for $80 \text{ K} < T < 300 \text{ K}$) were performed using a five-probe AC excitation technique [18]. The details of the experimental realization of the noise spectroscopy are given in earlier publications of the group [19–21]. Briefly, the noise was measured by recording the time series of voltage fluctuations $\Delta v(t)$ arising due to resistance fluctuation δR in a current biased ($I = 1 \mu\text{A}$) sample of resistance R . The voltage fluctuation times series ($\delta v(t)$) was measured by a phase-sensitive homodyne detection method. The homodyne mixed signal was demodulated by a lock-in-amplifier whose output was then digitized with a 16-bit analog to digital converter card of bandwidth 200 kHz. The frequency window of the noise spectrum in our experiment is $f_{\min} = 10$ mHz to $f_{\max} = 7$ Hz, which is the band width of detection. At each temperature, one data set was recorded with a sampling rate 1024 data points/s for nearly 16 minutes duration of data acquisition. Thus one data set contains about 1 million points. The stored data were decimated and digitally processed to obtain the power spectra [19]. The spectral power density was calculated from the stored and processed time domain data using method of average periodogram [22]. All the data were taken by stabilizing the temperature with accuracy ± 5 mK in heating cycle to avoid drift contribution to the fluctuation.

III. RESULTS

A. Structural data

Figure 1 shows the XRD and scanning probe microscopy data on the NNO film grown on BTO/STO (100). The XRD data show strongly oriented growth of BTO and NNO on

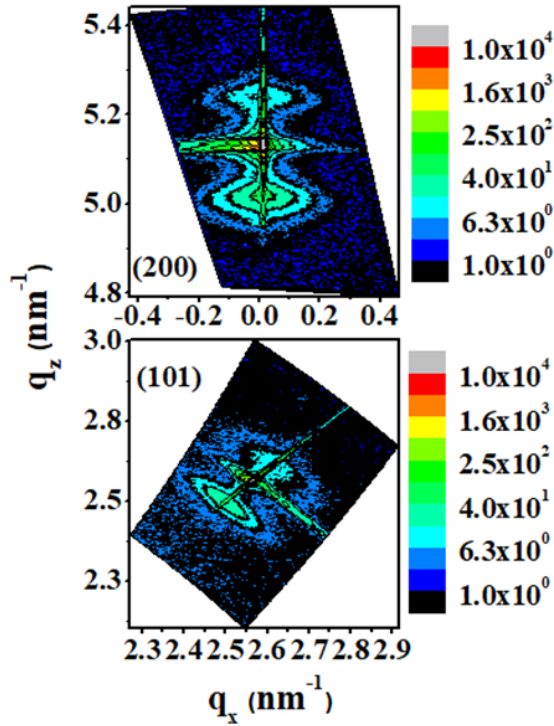


FIG. 2. Reciprocal space mapping (RSM) of the NNO/BTO/STO multilayer film using Cu $K\alpha$ radiation measured across the indicated reflections. The top, middle, and bottom lattice points corresponds to the NNO layer, STO substrate, and BTO layer, respectively.

STO (100). The (200) line being the most prominent line is highlighted. The NNO line and the BTO line straddle the STO line. The NNO line being at larger angle than the BTO line has smaller lattice constant compared to that of the BTO. The lattice constant of NNO film is $\approx 2.51\%$ smaller than that of STO and the BTO film is $\approx 2.18\%$ larger than that of the STO film. Thus, there is a large mismatch of lattice constant between NNO and BTO. The XRD scan shown in Fig. 1(a) covers the full 2θ range and shows absence of impurity peaks. The scanning probe microscope image [Fig. 1(b)] shows the surface morphology of the NNO film over a scan area of $1.3 \mu\text{m} \times 1.3 \mu\text{m}$ area. The film surface is highly compact with rms roughness of 1.6 nm. Scan shows growth of coherent grains of average grain size ~ 50 nm along the terrace steps of the substrate.

The growth of coherent grains as seen in the scanning probe microscope image occurs due to strain relaxation as established from the analysis of RSM data shown in Fig. 2. The analysis was carried out across the asymmetric (101) reflection. The data obtained from the analysis suggest relaxed states, which is reflected in the value of the relaxation parameter $R \simeq 0.99$. (Note: R is defined as $R = [(a_{\text{film}} - a_{\text{substrate}})/(a_{\text{film}}^R - a_{\text{substrate}})]$, a being the in-plane lattice constant. Subscripts film and substrate refer to film and the substrate, respectively. The superscript R refers to the fully relaxed film.) The out-of-plane strain (along c axis), $\epsilon_{\perp} = (c_{\text{film}} - c_{\text{film}}^R)/c_{\text{substrate}} = 0.51\%$, and in-plane strain (along a axis) $\epsilon_{\parallel} = (a_{\text{film}} - a_{\text{film}}^R)/a_{\text{substrate}} = -0.59\%$, as determined from RSM data. For the NNO film grown on BTO in the

NNO/BTO/STO (100) structure, the substrate parameters used are the measured parameters for BTO. The strain relaxation leads to the formation of misfit dislocations which are sources of quenched disorder and which also lead to strain inhomogeneity in the NNO film.

B. DC resistivity as a function of temperature

The DC resistivity ρ_{dc} vs T data taken during heating and cooling cycles are shown in Fig. 3(a). It can be seen that the high temperature metallic phase shows a bad metallic behavior with a high value of ρ_{dc} of 70 m Ω cm at room temperature. The TCR in this region $\frac{1}{\rho_{\text{dc}}} \frac{d\rho_{\text{dc}}}{dT}$ is < 0 . The derivative $\frac{d\rho_{\text{dc}}}{dT}$ data are shown in Fig. 3(b). The value of ρ_{dc} at 300 K corresponds to a conductivity $\sigma_{\text{dc}} = 14.3 \text{ S cm}^{-1}$, which is close to the Mott minimum conductivity value in many oxide systems [23,24]. In general, films of NNO grown on lattice matched substrates like SrTiO₃ (STO), LaAlO₃ (LAO), or NdGaO₃ (NGO) show much less resistivities at the room temperature which are $\approx 1\text{--}2$ m Ω cm [15,25,26]. These films with lower ρ show a good metallic behavior with $\frac{1}{\rho_{\text{dc}}} \frac{d\rho_{\text{dc}}}{dT} > 0$ and show a sharp MIT. Thus, in the NNO film grown on BTO, the MI transition is a transition from a bad metal to an insulator and it shows a broad nature.

There is a sharp rise of the resistivity at the lowest temperature of measurement ($T = 4$ K) as can be seen in Fig. 3(a). The rise is caused by a time-dependent relaxation of the resistance which occurs when the temperature is held constant at 4 K. The resistance relaxation is related to relaxation of small supercooled portion of high temperature metallic phase (that has lower resistivity) to the low-temperature (equilibrium) insulating phase (that has higher resistivity) when the NNO film is cooled below the stability temperature of supercooling, which is $< T_{\text{MI}}$. We had cooled down the sample to 4 K with a fixed ramp rate 2 K/min and waited for around one hour till the resistance relaxation is complete [Fig. S2(b)] [27] and it reaches the equilibrium value for the low-temperature insulating phase. When it is warmed up again (with same ramp rate of 2 K/min), it follows an equilibrium curve as shown in Fig. 3(a). The supercooling phenomena have been observed previously in rare-earth nickelates [28,29]. The supercooling and the low temperature relaxation have no influence on the phenomena reported here, which occurs in the temperature range above T_{MI} where the system is in equilibrium. All the data were taken during the heating cycle after the sample has been cooled to 4 K, equilibrated, and then warmed up at a slow rate

The resistivity of the bad metallic state can be fitted to the relation $\rho_{\text{dc}}(T) = \rho_{0m} - \rho_1 T$, where ρ_{0m} and ρ_1 are constants (see Fig. S1) [27]. Finite nonzero value of $\rho_{0m} = 0.11 \Omega \text{ cm}$ and the absence of an activated-type temperature dependence suggests that large disorder in the NNO film grown on BTO drives it close to a disorder-driven Anderson transition. It has been shown by our group that in a substitutionally doped Nd_{1-x}La_xNiO₃ ($x = 0.3$), there can be a continuous transition from a weakly localized regime to a strong localization regime tuned by substrate-induced strain [24].

In the insulating state at the low-temperature limit ($T \gg T_{\text{MI}}$), the DC resistivity follows variable range hopping relation: $\frac{\rho}{T^{1/4}} = \rho_0 \exp(\frac{T_0}{T})^{1/4}$ for $T \leq 10$ K. (Fit to data are

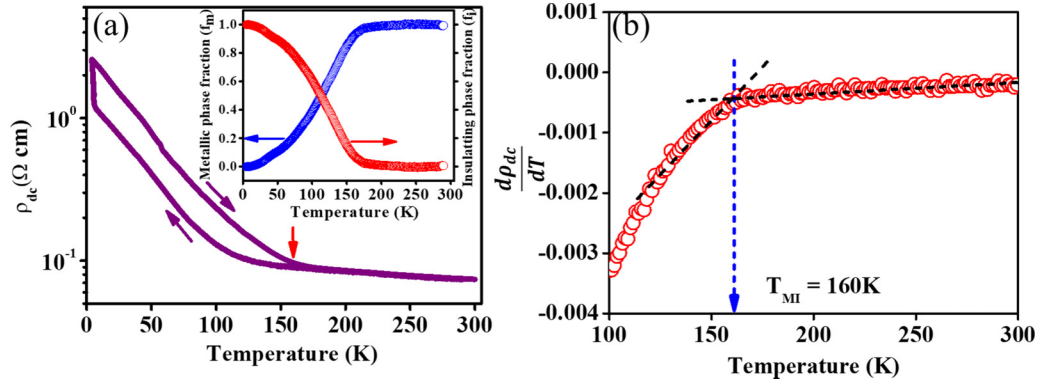


FIG. 3. (a) Resistivity of the NNO film grown on BTO/STO as a function of temperature. Inset shows the metallic and insulating phase fractions obtained from the resistivity data (heating cycle). (b) Derivative of DC resistivity $\frac{d\rho_{dc}}{dT}$ vs T . The MIT temperature T_{MI} is marked by an arrow. Data taken during heating cycle

shown in Fig. S2 (a) [27]). Since the MIT occurs from a bad metallic state to an insulating state, both of which have $\frac{d\rho_{dc}}{dT} < 0$, the exact location of the MIT temperature (T_{MI}) has an element of uncertainty which is often done through the change of signs of the derivative, as has been shown in Fig. 3(b). Sometimes T_{MI} can be better identified from the conductivity $\sigma_{dc}(\equiv \frac{1}{\rho_{dc}})$ vs T plot (see Fig. S3) [27]. From these data, we locate the $T_{MI} = 160$ K.

In the whole temperature range, the resistivity data can be fitted by an effective medium approximation with two limiting phases at high and low temperatures, respectively [30]. The inset in Fig. 3(a) shows the metallic (f_m) and insulating fractions (f_i) as functions of temperature obtained from fitting the resistivity data taken during the heating cycle. The insulating fraction $f_i \approx 0.1$ at T_{MI} . The coexisting phases near the MIT makes the transition broad and adds a percolative nature to the transition where the relative metallic and insulating phase fractions continuously change with T . If we roughly define the transition width as the temperature region where the insulating phase fraction goes from 90% to 10%, the width is found to be ≈ 50 K. The data show the diffused nature of the MI transition due to disorder that leads to significant broadening of the transition region. This is unlike the sharper transitions seen

in films of NNO grown on STO, LAO, or NGO that shows the first-order nature of the transition.

C. Low frequency noise spectroscopy

Noise spectroscopy is a sensitive probe of the MIT, in particular, when there are coexisting phases. Past reports of $\frac{1}{f}$ noise spectroscopy near the MIT in rare-earth nickelates like NNO and SmNiO_3 have established the emergence of substantial low-frequency correlated fluctuations at $T \approx T_{MI}$ [15,31–33]. In this paper, we show that use of noise spectroscopy identifies not only the MIT temperature T_{MI} but very importantly it marks clearly another temperature T_G above T_{MI} , where slow dynamics of relaxation sets in and the low-frequency dynamics persists over a distinct temperature region $T_{MI} < T < T_G$. It is noted that in the previous noise spectroscopy studies in oxides undergoing MI transition, existence of such a temperature has not been identified and reported.

The spectral power density of flicker follows the relation $\frac{S_V(f)}{V^2} \propto \frac{1}{f^\alpha}$. The exponent α was obtained from the frequency-dependent spectral power density data by nonlinear least squares fit. This is shown in Fig. 4(a), where the data are shown in double-log plot of the scaled spectral power density

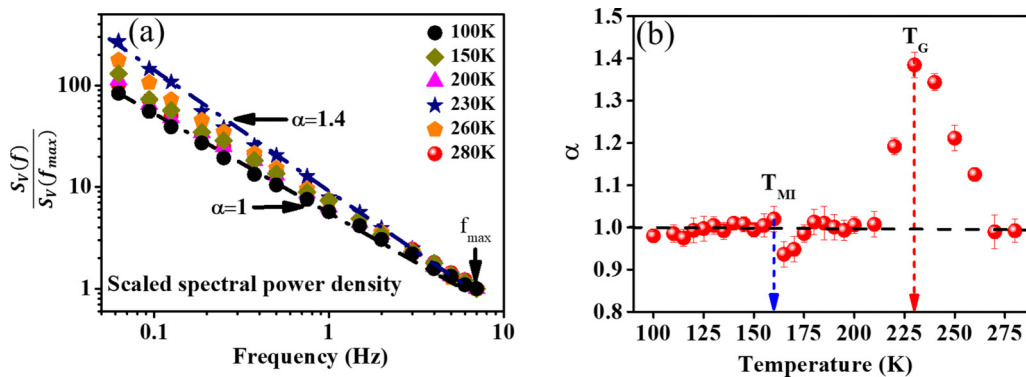


FIG. 4. (a) Scaled spectral power density $\frac{S_V(f)}{S_V(f_{max})}$ as a function of frequency f in NNO/BTO/STO at few representative temperatures. (b) The exponent α for the spectral power density ($S_V \sim \frac{1}{f^\alpha}$) as a function of T . α shows a prominent peak at the temperature T_G marked by red arrow. Away from $T_G \alpha \approx 1$. No discernible feature is seen near T_{MI} (marked by blue arrow). The enhancement of α to 1.4 near T_G can be seen in (a).

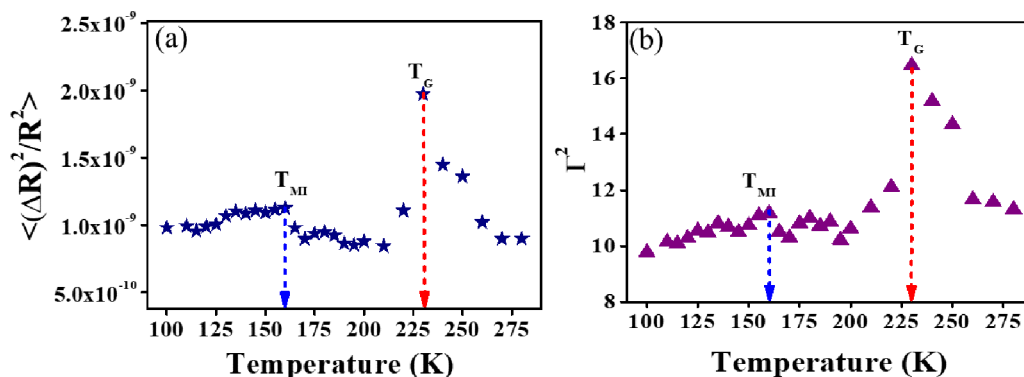


FIG. 5. (a) Temperature dependence of relative variance of fluctuation $\langle \frac{\Delta R^2}{R^2} \rangle \equiv \frac{1}{V^2} \int_{f_{\min}}^{f_{\max}} S_V(f) df$. (b) The second spectrum Γ^2 of the noise spectra as a function of temperature. The temperatures T_{MI} and T_G are marked.

$\frac{S_V(f)}{S_V(f_{\max})}$ with frequency f . $\frac{S_V(f)}{S_V(f_{\max})}$ is the spectral power density at a frequency f scaled by its value at $f_{\max} = 7$ Hz, which is the maximum of the bandwidth of measurement. As the temperature changes, the exponent α evolves nonmonotonically, as shown in Fig. 4(b). It can be seen that the exponent α shows clear enhancement at a well-defined temperature T_G marked by an arrow and it deviates from the value of ≈ 1.0 as T_G is approached from both above or below. The width of the temperature range around T_G where α shows significant deviation from the value of 1.0 is ≈ 50 K. Away from this range, $\alpha \sim 0.95$ – 1.0 as is expected of a conventional flicker noise [19,34]. The change in the exponent α can be appreciated from Fig. 4(a) as well. For T away from T_G , the exponent $\alpha \approx 1$ as can be appreciated from the dotted line that has $\alpha = 1$. As $T \rightarrow T_G$, the exponent $\alpha \rightarrow 1.4$ as can be seen from the enhanced slope of the line marked in the figure. This is a change in the value of α by nearly 40%. Change of α from 1 to 1.4 indicates that the spectral weight has shifted to lower frequency. It may be noted that α generally has a limited range typically from 1 to 2 as observed from various systems [19].

Figure 5(a) shows the temperature dependence of the normalized mean square resistance fluctuation $\langle \frac{\Delta R^2}{R^2} \rangle \equiv \frac{1}{V^2} \int_{f_{\min}}^{f_{\max}} S_V(f) df$, where the integral is over the band width of measurement (f_{\min} , f_{\max}). (The normalized mean-square fluctuation is often referred to as magnitude of noise). The data show that while there is a broad and shallow hump in the noise magnitude in the temperature range $T \sim T_{MI}$, it rises sharply as the temperature T_G is approached from both above and below, where there is appearance of large component of low frequency fluctuation as inferred from the sharp rise in the exponent α . It can be seen from Fig. 5(a) that at T_G the value of the normalized mean square fluctuation changes substantially by a factor of 2 from its value away from T_G . Figures 4(b) and 5(a) clearly establish that a large low-frequency fluctuations arises in the temperature range $T_{MI} < T < T_G$, as $T \rightarrow T_G$.

The large low-frequency fluctuations that appear in the temperature range $T_{MI} < T < T_G$, are non-Gaussian. It can be seen in Fig. 5(b) that the value of the second spectrum Γ^2 changes from 10 to nearly 17 at $T = T_G$. This would be expected when the noise sources from which the fluctuations arise are correlated in nature. Correlated fluctuation and its non-Gaussian nature have been measured through the normal-

ized second spectrum given by [15,19,21]

$$\Gamma^2 = \int_0^{f_H - f_L} S^{(2)}(f_2) df_2, \quad (1)$$

where

$$S^{(2)}(f_2) = \frac{\int_0^\infty \langle \Delta v^{(2)}(t) \Delta v^{(2)}(t + \zeta) \cos(2\pi f_2 \zeta) d\zeta}{\left[\int_{f_L}^{f_H} S_V(f_1) df_1 \right]^2}, \quad (2)$$

where f_1 and f_2 are the frequencies associated with first and second spectra, respectively. $\Delta v(t)$ is the measured voltage fluctuation.

Observation of a distinct temperature T_G above T_{MI} which marks the onset of slow relaxation in the system that shows diffused MIT is one of the principal observations of the paper. This occurs at a temperature range where the metallic phase is the majority phase with a very small fraction of insulating phase ($f_i \approx .001$). The temperature range $T_{MI} < T < T_G$ is also distinct where the low-frequency fluctuation is correlated as judged from its non-Gaussian nature.

D. AC conductivity and impedance spectroscopy

The noise spectroscopy data point toward the emergence of behavior at temperature T_G which is distinct from the temperature T_{MI} . It will be of interest to investigate the transition region with another independent dynamic probe to explore whether a signature of T_G can be found. In the region of temperature where T_G occurs, the minority phase fraction being very small, it is not observable in DC resistivity measurements. Thus, there is a need for a dynamic probe like IS that may capture the presence of small regions of a minority phase in a solid with coexisting phases.

The temperature-dependent DC resistivity data suggest coexisting phases near the MIT, which has also been observed in our previous experiment on NNO grown on lattice-matched LAO where coexisting phases have been detected directly through scanning tunneling spectroscopy data [15]. In such coexistence regions, the charge relaxation will be determined by conductivities of the coexisting regions where metallic regions of higher conductivity separated by an insulating region will show a capacitive effect which will control the complex impedance.

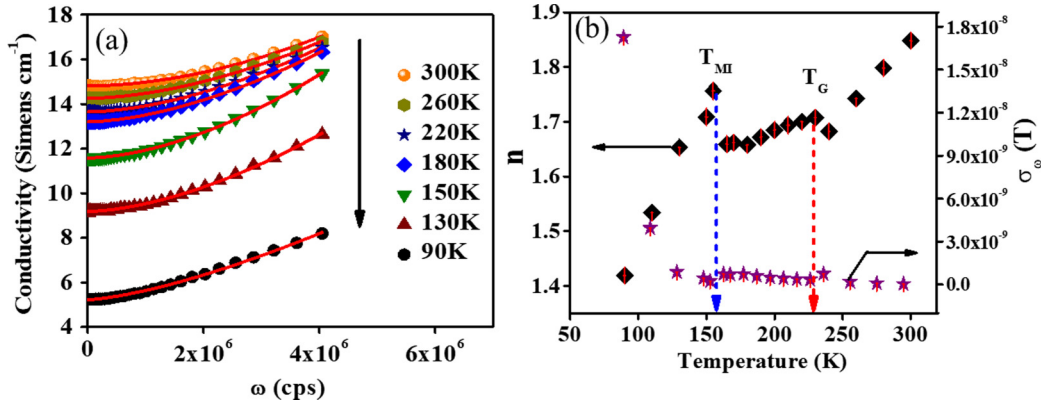


FIG. 6. (a) AC conductivity $\sigma(\omega, T)$ of the NNO film grown on BTO/STO as a function of frequency ω at a few selected temperatures T . Fits to Eq. (3) are shown as line. (b) Variation of the exponent $n(T)$ and $\sigma_\omega(T)$ as a function of T . Two temperatures T_{MI} and T_G are marked by arrows.

The AC conductivity ($\sigma(\omega, T)$) was measured as a function of frequency $\omega = 2\pi f$ at different temperatures down to 80 K. The data were taken in a planar configuration where the current is in plane of the film and are shown in Fig. 6(a). To estimate the frequency-dependent part, the data in Fig. 6(a) were fitted to the phenomenological relation:

$$\sigma(\omega, T) = \sigma(\omega = 0, T) + \sigma_\omega(T)\omega^{n(T)}. \quad (3)$$

The AC conductivity $\sigma(\omega, T)$ vs T data were fitted to Eq. (3) using nonlinear least-squares fit. Parameters $\sigma(\omega = 0, T)$, $\sigma_\omega(T)$ and the exponent $n(T)$ were taken as fit parameters. The value of $\sigma(\omega = 0, T)$ as obtained from the fit is $\approx \sigma_{dc}(T)$, which has been obtained experimentally in Sec. II B establishing correctness of the fit procedure. The solid lines through the data points in Fig. 6(a) are the fits to Eq. (3). Temperature variations of the exponent $n(T)$ and $\sigma_\omega(T)$ by fitting the AC conductivity data to Eq. (3) are shown in Fig. 6(b). The temperature dependence of both parameters clearly shows signatures of the MIT temperature T_{MI} . To appreciate the change in the frequency-dependent part, we show $\sigma(\omega, T) = \sigma(\omega = 0, T)$ as a function of ω at different T in Fig. S9 [27]. The variation in $n(T)$ with T can be appreciated as $T \rightarrow T_{MI}$. The enhancement of the frequency-dependent part $\sigma_\omega(T)$ below T_{MI} is opposite to the temperature dependence of $\sigma(\omega = 0, T)$. This implies significant rise of the relative contribution of the frequency-dependent part of AC conductivity in the low-temperature insulating phase. The temperature variation of $\sigma(\omega = 0, T)$, as expected, mimics that of the measured DC conductivity σ_{dc} . Interestingly, the exponent $n(T)$, shows a nonmonotonous behavior with very discernible breaks at both temperatures T_{MI} as well as T_G . The observed feature in $n(T)$ at temperature T_G does signal the onset of a new regime of precursors to the MIT. In this context, it will be interesting to compare the AC conductivity data obtained on the film NNO grown on STO (NNO/STO) that does not show any anomalous feature outside the range of T_{MI} . The data for NNO/STO are shown in Fig. S4(a) [27]. The corresponding variation of $n(T)$ and $\sigma_\omega(T)$ are shown in Fig. S4(b) [27]. The sharp changes in the parameters seen for NNO/BTO/STO above T_{MI} are absent in those of the film NNO/STO. Later, in the Discussion section we undertake an analysis of the AC conductivity data with a model of coexisting phases and show

that the features seen in the range $T_{MI} < T < T_G$ arise from a change in the size distribution of conducting clusters.

Figure 7 shows the plot of the imaginary part of the impedance Z'' versus the real part Z' at a given frequency (Cole-Cole plot) for NNO film grown on BTO at a few representative temperatures spanning the temperatures T_{MI} as well as T_G . The lines through the data are fits using a simple phenomenological model equivalent circuit whose schematic is shown in the inset of Fig. 7. The model is a parallel combination of resistance R_2 and C_{obs} in series with a resistance R_1 [see Eq. (4)]. To fit the impedance data to the phenomenological model, we used the software EIS Spectrum Analyser. EIS Spectrum Analyser is a stand-alone program for analysis and simulation of impedance spectra [35]. The data file of the as-observed impedance data of real part (Z') and imaginary part (Z'') as a function of frequency were used as inputs in the software. All three parameters (R_1, R_2, C_{obs}) have been initialized automatically and were approached toward the best fit by multiple iterations.

Impedance measurements were done in a planar geometry with field and the current in the film plane. $C_{obs}(T)$ in the model is a lumped temperature-dependent (but frequency-independent) parameter that is an equivalent capacitance in

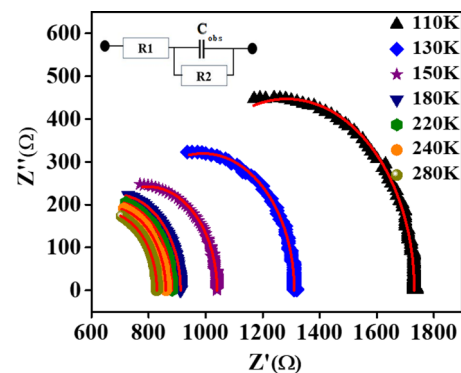


FIG. 7. Cole-Cole plot of impedance data at few representative temperatures. The line through the data are fits to the impedance data using a model equivalent circuit whose schematic is shown in the inset.

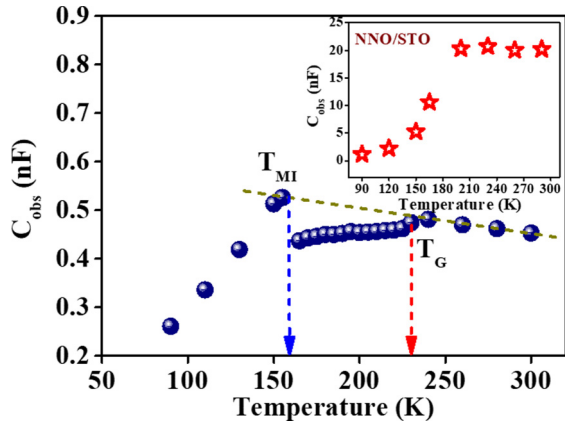


FIG. 8. Temperature variation of the capacitance parameter $C_{\text{obs}}(T)$ of the NNO film grown on BTO/STO. The MI transition temperature T_{MI} and the temperature T_G observed in noise data are also marked. The dotted line is a simple extrapolation to show expected behavior of $C_{\text{obs}}(T)$ in absence of a T_G . The inset shows the capacitance of the NNO film on STO.

the film. The complex impedance data $Z(\omega, T)$, based on the simple model above, are given by the relation

$$Z(\omega, T) = Z' + iZ'' = R1 + \frac{R2(T)}{1 + j\omega R2(T)C_{\text{obs}}}. \quad (4)$$

In the model above, the resistances $R1$ and $R2$ as well as $C_{\text{obs}}(T)$ were assumed to have no explicit frequency dependence. This assumption is justified because the contribution of the frequency-dependent term of the AC conductivity $\sigma_{\omega}(T)\omega^{n(T)}$ is quite small compared to the frequency-independent term $\sigma(\omega = 0, T)$ for $\omega \leq 10^6$ cps. This can also be appreciated from Fig. 6(a). Based on the above, the lumped resistances $R1$ and $R2$ are assumed to be frequency independent. $C_{\text{obs}}(T)$ has been assumed to be frequency independent mainly to obtain a scale for the capacitance. The frequency-independent $C_{\text{obs}}(T)$ corresponds to an average capacitance at a mean frequency $\omega_0(T)$ discussed later in Sec. IV A along with Eqs. (5) and (6). $C_{\text{obs}}(T)$ as a function of T , as obtained by fitting the impedance data, are shown in Fig. 8. A sharp jump is observed at $T \approx T_{\text{MI}}$ and also another prominent break in slope with a shallow peak is observed at $T = T_G$. The $R1$ and $R2$ data are given in Fig. S5 [27]. Both show a rapid rise on cooling below T_{MI} and show a break in slope at $T = T_G$. (see insets of Fig. S5) [27].

The temperature dependence of $C_{\text{obs}}(T)$ for NNO/BTO is distinct from that of $C_{\text{obs}}(T)$ seen in NNO/STO (see the inset in Fig. 8 which shows a decrease that starts around T_{MI} but shows no discernible T_G). The temperature dependence of $C_{\text{obs}}(T)$ seen in NNO/STO is similar to that also seen in NNO/LAO [15]. For both NNO/STO and NNO/LAO, $C_{\text{obs}}(T)$ as a function of T show a broad peak at T_{MI} followed by a distinct fall. In contrast, in NNO/BTO, the rise of $C_{\text{obs}}(T)$ at T_{MI} as it is approached from above is interrupted by the existence of the temperature range $T_{\text{MI}} < T < T_G$ where there is a distinct decrease in $C_{\text{obs}}(T)$ on cooling followed by a jump at T_{MI} . We show the expected behavior of $C_{\text{obs}}(T)$ as a function of T in Fig. 8 by the dotted line which would have occurred had there been no T_G and no intervening phase in the

temperature range $T_{\text{MI}} < T < T_G$. The distinct feature seen in the equivalent capacitance in this temperature range signals the existence of a different nature of coexisting phases, that is different from both the insulating phase below T_{MI} and the metallic phase above T_G .

The capacitance in the transition region arises due to coexisting phases of differing conductivities where charging of the conducting phase (isolated by insulating phase) leads to capacitance of the film. The temperature variation leads to a change in the relative volume fraction of the two phases, leading to temperature dependence of the capacitance. The value of the capacitance depends on the relative conductivities of the two phases which in effect decides the interfacial charges in the region between two phases. For the NNO film grown on lattice-matched STO, the metallic phase has much lower resistivity, leading to a larger relative difference of the two coexisting phases and larger capacitance of the film. In contrast, in the NNO film grown on BTO, due to strain relaxation and quenched disorder as pointed out earlier, the high-temperature phase is a bad metallic phase with a resistivity that is much larger. This results in suppression of the relative conductivities of the two coexisting phases, which in turn leads to less effective capacitance of the NNO/BTO/STO film. The distinct feature seen in the equivalent capacitance in this temperature range signals the existence of a different nature of coexisting phases that is different from both the insulating phase below T_{MI} and the metallic phase above T_G .

E. Correlation function of fluctuations and the correlation time

If slow kinetics of relaxation leads to large flicker noise as well as a large value of the exponent α in the MIT transition region, then it is expected that the correlation time of fluctuation (τ) will also show enhancement. τ is directly obtained from the autocorrelation function $\phi(t)$ of the voltage fluctuations [19]. We show that τ has a distinct temperature dependence and it shows a maximum at T_G , where the flicker noise shows a peak along with large value of the exponent α .

The autocorrelation function $\phi(t)$ is defined as $\phi(t) \equiv \langle \delta v(t')\delta v(t+t') \rangle_{t'}$, where $\langle \dots \rangle_{t'}$ represents the time average and $\delta v(t)$ is the observed times series of voltage fluctuation. $\phi(t)$ shows an approximate exponential dependence for small time ($t \leq \tau$) and a long-time tail for $t > \tau$. Data for $\phi(t)$ at some representative temperatures are shown in Fig. 9(b). The dashed line in Fig. 9(b) demarcates the exponential region and the nonexponential long-time tail. We obtain the correlation time τ approximating it as the time when $\phi(t)$ becomes $\frac{1}{e}$ of the value at $t = 0$. The long-time tail of $\phi(t)$ contains valuable information on the nature of the coexisting phases in the region $T_{\text{MI}} < T < T_G$ and will be discussed separately in the next section.

In Fig. 9(a), we show the temperature dependence of τ as obtained from the correlation function. It can be seen that the correlation time gradually increases as T_G is approached either from above or below and it shows a peak at $T = T_G$. The value of τ at the peak is about a factor of 2 larger than that at temperatures away from T_G . The significant enhancement of τ at $T = T_G$ thus corroborates with the appearance of large low-frequency noise in the same temperature range.

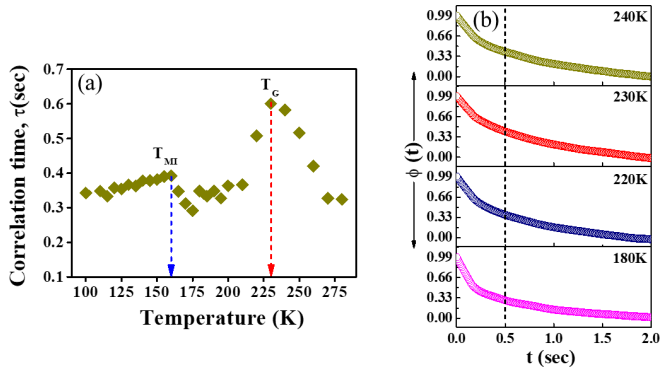


FIG. 9. (a) Temperature dependence of τ as obtained from the correlation function and (b) correlation function $\phi(t)$ vs t at some representative temperatures in the range $T_{MI} < T < T_G$. The dashed line demarcates the exponential region and the nonexponential long timescale.

To summarize the main results, we find that in the film NNO grown on BTO/STO (100) that has significant lattice mismatch with BTO, there is a MIT, albeit from a bad metal with high resistivity to an insulator whose resistance follows a temperature dependence given by variable range hopping. The transition has a percolative nature where the metallic and insulating fractions are temperature dependent. The disorder severely broadens the transition region making the transition a diffuse transition rather than a sharp MIT.

Importantly, we find that above the transition temperature T_{MI} , there are clear signatures of existence of another temperature T_G identifiable by noise spectroscopy as well as by impedance spectroscopy, which signals the onset of correlated low-frequency fluctuations and the onset of slow dynamics. We discuss in next section that T_G may be identified with the onset of an electronic Griffiths phase. We emphasize that past noise spectroscopy investigations done on oxides undergoing Mott-type MITs have reported the appearance of large correlated low-frequency fluctuations. However, no study to date in such oxides reported a distinct temperature like T_G which shows the onset of a temperature region where slow relaxation sets in as a precursor to MI transition. This observation corroborates a recent report of such a temperature regime above the MI transition temperature in organic systems which have been identified as the onset of an electronic Griffiths phase [4,12].

IV. DISCUSSION

A. Broad transition region and coexisting phases

The diffused nature of the MIT in the NNO/BTO shows anomalous features in the AC conductivity $\sigma(\omega, T)$ in the region of temperature $T_{MI} < T < T_G$. This is reflected in the anomalous temperature-dependent behavior of the exponent $n(T)$ [refer to Eq. (3)]. The AC conductivity in many electronic systems including oxides with disorder, doped semiconductors, polymers, and composite solids follow a power law given by Eq. (3). The exponent $n(T)$ contains information on the hopping character of the charge carriers through localized states and it depends on the morphology

of the conducting path [36]. In general, $0 < n < 1$ at low frequencies and changes over to $1 < n < 2$ at higher frequencies. Mott's theory suggests that in insulating systems with localized states $n \rightarrow 2$. The crossover from $n < 1$ to $n > 1$ can occur in THz frequency range, although there are reports in the context of oxides that the crossover can occur at KHz range as well [36]. In the present paper, we find that in the whole temperature range the data fits with an exponent n , which lies in the region $1 < n < 2$ and decreases on cooling and which shows anomalous features in the temperature range $T_{MI} < T < T_G$. A detailed discussion on the nature of the exponent is beyond scope of the paper. However, we note that the presence of coexisting phases distinct from both the low-temperature insulating phase and the high-temperature metallic phase are indicated by the behavior of n . As elaborated below, we analyze the AC conductivity data using a model of coexisting phases comprised of a size distribution of metallic clusters.

The model [37] had been proposed to understand that conductivity of a composite medium with coexisting insulating and metallic phases with a distribution of conducting region size (ξ) as happens close to a MI transition. In this model, the frequency dependence arises as a consequence of the distribution in ξ . The length scale ξ of the conduction region determines the timescale of charge diffusion and hence the frequency dependence through the relation $\xi \approx \sqrt{D/\omega}$, where D is a typical mean carrier diffusivity. The total conductivity consisting of the DC conductivity and the frequency-dependent part of the conductivity that consists of contribution from the conducting regions. This is given as [37]

$$\sigma(\omega, T) = \sigma_{dc} + A(T) \int_0^\omega \frac{1}{(2\pi)^{1/2} \Sigma} \times \exp\left(-\frac{(\log_{10}\omega - \log_{10}\omega_0)^2}{2\Sigma^2}\right) d\omega, \quad (5)$$

where the length scale has a log-normal distribution with width Σ and most probable length scale ξ_0 that defines $\omega_0 = \frac{D}{\xi_0^2}$. The constant $A(T)$ has the dimension of conductivity and contains geometric factors. Both parameters $\Sigma(T)$, $\omega_0(T)$ are temperature dependent. Smaller metallic regions that cannot take part in charge transport would contribute to the capacitance, which is given as [37]

$$C(\omega, T) = C_0(T) \int_\omega^\infty \frac{1}{(2\pi)^{1/2} \Sigma} \times \exp\left(-\frac{(\log_{10}\omega - \log_{10}\omega_0)^2}{2\Sigma^2}\right) d\omega, \quad (6)$$

where $C_0(T)$ is a frequency-independent scale for the capacitance.

The observed $\sigma(\omega, T)$ data were used to fit them to Eq. (5) and obtain the relevant parameters. The parameters in Eq. (5) were fixed as follows. The measured DC resistivity data as shown in Fig. 3(a) was used for $\sigma_{dc}(= \frac{1}{\rho_{dc}})$. The average characteristic relaxation frequency for a cluster $\omega_0(T)$ at each temperature T sets the scale for the frequency-dependent part of the AC conductivity. The value of $\omega_0(T)$ was estimated from the observed frequency-dependent part given as $\omega_0(T) \equiv \left(\frac{\sigma(\omega=0, T)}{\sigma_\omega(T)}\right)^{\frac{1}{n(T)}}$, where these parameters were

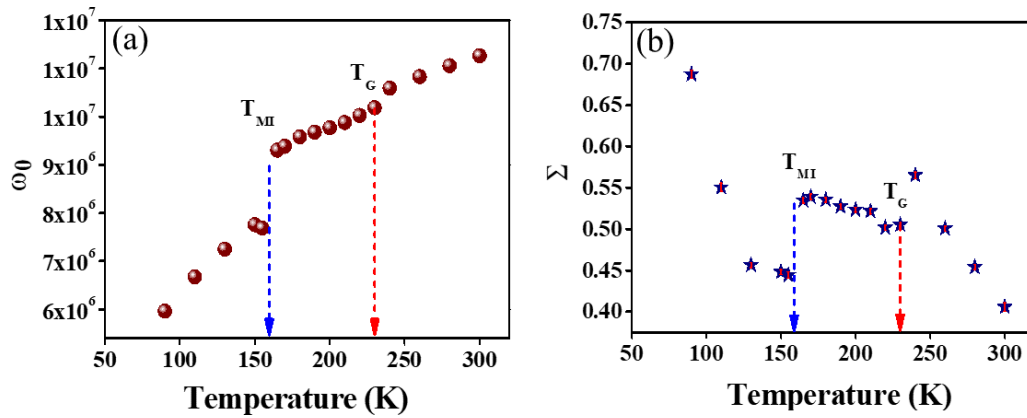


FIG. 10. (a) Temperature dependence of the parameter $\omega_0(T)$ and (b) $\Sigma(T)$.

obtained directly from fit of the AC conductivity data to Eq. (3) discussed before. The parameters $A(T)$ and $\Sigma(T)$ were used as fit parameters for each T . The fitting has been carried out in the MATLAB platform using existing packages for least-squares fit. The quality of fits of Eq. (5) to the data are shown in Fig. S6 in the Supplemental Material [27]. The values of the parameters $\omega_0(T)$ and $\Sigma(T)$ obtained from fitting are shown in Figs. 10(a) and 10(b), respectively. ω_0 shows a decrease on cooling with a change in slope at T_G . It shows a perceptible jump to a much lower value at T_{MI} . The width of distribution $\Sigma(T)$ also shows an enhancement on cooling but shows a break from the monotonous behavior at both T_G and T_{MI} with signature of a different behavior in the range $T_{MI} < T < T_G$ that corroborates with the observations made from the noise data. The factor $A(T)$ has a soft temperature dependence and shows a shallow peak at $T \sim T_G$ as shown in Fig. S7 [27].

We have determined the frequency- and temperature-dependent capacitance $C(\omega, T)$ using Eq. (6). The frequency-independent constant $C_0(T)$ in Eq. (6) was obtained by equating $C_{obs}(T)$ to $C(\omega_0, T)$ at each T . This assumes that $C_0(T)$ is an average capacitance at the mean frequency ω_0 . Both the parameters $\Sigma(T)$, $\omega_0(T)$ used in calculation of $C(\omega, T)$ using Eq. (6) have been obtained from fit of the AC conductivity data to Eq. (5) as elaborated before. A contour plot of $C(\omega, T)$ is shown in Fig. 11. $C(\omega, T)$ obtained from Eq. (6) is shown in Fig. S8 as a function of ω at different T [27].

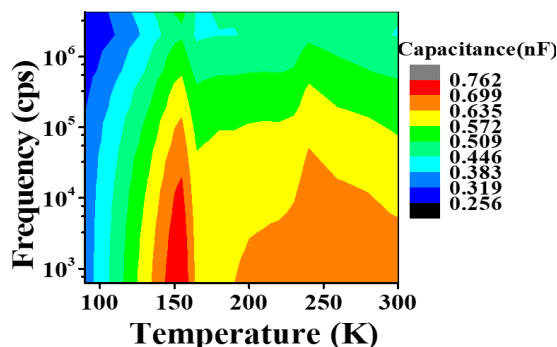


FIG. 11. A contour plot of $C(\omega, T)$ evaluated from Eq. (6).

Figures 11 and S8 [27] show that the capacitance for a given frequency has regions of high value at $T \sim T_G$ and at around T_{MI} . The frequency dependence of $C(\omega, T)$ is a point in question. It shows explicit frequency dependence of the capacitance which was missing from the simple RC model shown before. The decrease in the capacitance at higher frequencies would imply lower fraction of very small conducting pockets.

Variation of ω_0 as shown in Fig. 10(a) reflects the reduction in diffusivity D of carriers as the temperature is changed. Since $\omega_0 = \frac{D}{\xi_0^2}$, a sudden lowering ω_0 at T_{MI} would signify a sudden reduction in D at the onset of the insulating phase and it reduces precipitously as the temperature is reduced further. The anomalous variation in Σ reflects the change in the distribution in the frequency as it becomes broader below the transition and shows a rather flat temperature dependence in the temperature range $T_{MI} < T < T_G$.

B. Likely signature of onset of Griffiths phase at T_G

We explore the feasibility whether the temperature T_G can be identified as the onset of an electronic Griffiths phase. The concept of a magnetic Griffiths phase has been explored experimentally extensively, particularly in doped rare-earth manganites that show colossal magnetoresistance [38–44]. In the temperature range between T_G and T_{MI} , the system is a like a composite of the high-temperature bad metallic phase and low-temperature insulating phase, very similar to the situation for magnetic Griffiths phase where below an onset temperature the disordered paramagnetic state coexists with a local ferromagnetically ordered phase. As a result, the magnetic Griffiths phase contains small ferromagnetic clusters embedded in the paramagnetic phase.

In a very recent publication, electronic Griffiths phase has been reported in organic solids (with disorder) that show Mott transition [12]. The paper concludes the occurrence of an electronic Griffiths phase in a system with slow fluctuations in electrons close to the Mott-insulator boundary in the presence of quenched disorder. The onset of slow (and correlated) fluctuations observed in the present investigation around temperature T_G and its presence over the temperature range $T_{MI} < T < T_G$ would thus be evidence that T_G may

be identified as the onset temperature of Griffiths phase in correlated electron systems.

The NNO films grown on BTO as discussed before is not coherently strained but strain relaxed with residual strain as can be judged from rather large value (-0.59%) of in-plane strain ϵ_{\parallel} (%). The strain relaxation in the film would give rise to misfit dislocations. The appearance of grains in the films (with grain boundaries) as shown in Fig. 1(b) would give rise to concomitant strain inhomogeneity. From the high-resolution x-ray data, we obtained the rocking curve of the NNO film. From the rocking curve, the full width at half maximum (FWHM) was evaluated to be $\approx 2^{\circ}$. The value of the FWHM is large and points to significant strain inhomogeneity in the film that would arise from quenched disorder. Thus, in the NNO film on BTO there is quenched disorder which leads to a bad metallic phase as seen through the high value of resistivity ρ and a negative $\frac{d\rho}{dT}$. As a consequence, the appearance of a Griffiths phases above T_{MI} is a likely proposition [12].

The Griffiths phase needs the coexistence of phases which the film under investigation shows near the transition region. It has been proposed [11] that the appearance of a Griffiths phase above the MIT temperature T_{MI} would need an occurrence of sparse phases like small pockets of the high-temperature phase embedded in pockets of minority low-temperature phases which in turn are dispersed in the majority high-temperature phase. In the temperature region around T_G , the insulating phase is the minority phase with phase fraction $f_i \ll 1$. Thus, small pockets of the metallic phase embedded in the minority insulating phases will be very rare and will occur over a small temperature region between T_G and T_{MI} . At higher temperature ($T > T_G$), the growing metallic phase will subsume the small pockets of insulating phases in which the sparse metallic phase is embedded, and at much lower temperatures below the MI transition, the growing insulating phase will subsume the high temperature phase. Occurrence of such a sparse phase will lead to slow relaxation kinetics as has been observed experimentally. Theoretical investigations established that these rare regions can control the long-time dynamics in a Griffiths phase. As a result, the autocorrelation function $\phi(t)$ of the fluctuation has a predominant low-frequency contribution. This will lead to a long-time tail which would vary as [11]

$$\phi(t) \sim \exp(-\phi_c (lnt)^{\frac{d}{d-1}}), \quad (7)$$

where ϕ_c is a constant and d is the dimension. For $d = 3$, one would expect the long-time tail of $\phi(t)$ to vary as $\phi(t) \sim \exp(-\phi_c (lnt)^{\frac{3}{2}})$. We find that $\phi(t)$ in the system does grow a long-time tail following Eq. (7) as shown in Fig. 12, where the time axis has been scaled by the correlation time τ , which allows scaling of the correlation functions at different temperatures to be represented in a single scaled graph. The solid lines through the data points are fit to Eq. (7) for $d = 3$. The proposal of the existence of a sparse phase and the long tail correlation function provides strong support for the hypothesis that the temperature T_G is analogous to the onset temperature of the Griffiths phase as observed in magnetic phase transitions.

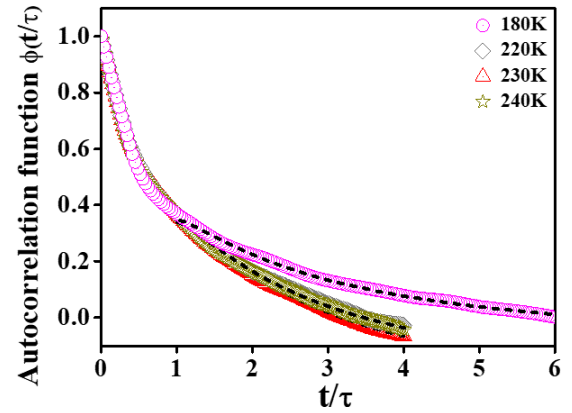


FIG. 12. Time dependence of the scaled autocorrelation function for fluctuation $\phi(\frac{t}{\tau})$ versus scaled time $\frac{t}{\tau}$ at a few temperatures close to T_G . The dashed line through the data at longer times ($\frac{t}{\tau} \geq 1$) shows fit to Eq. (7).

V. CONCLUSION

NNO film grown on a substrate BTO/STO (with large mismatch of lattice constant) shows a Mott-type MIT at a temperature $T_{MI} = 160$ K from a high temperature bad metallic phase with high value of resistance $=70$ m Ω cm (at 300 K) and a negative TCR to a low temperature insulating phase. The bad metallic phase is similar to what is expected in an oxide with quenched disorder close to the disorder driven Anderson transition [23]. Such a bad metallic phase is not observed in NNO when the films are grown on crystalline substrate like STO that have better matching with lattice constants. The MIT in presence of disorder has a percolative nature with coexisting phases not only close to the transition region but also away from it thus making the transition a broad one.

Using noise spectroscopy and IS that probe the dynamics of the coexisting phases, it was observed that in addition to the MIT at a temperature T_{MI} , there exists a characteristic temperature T_G above T_{MI} which signals onset of a temperature region $T_{MI} < T < T_G$ where new features are observed. The observed features show the emergence of large low-frequency correlated fluctuations signifying the onset of a phase with slow dynamics. The new phase in the region $T_{MI} < T < T_G$ likely arises from small clusters of metallic phase embedded in pockets of insulating phases that coexist with the majority high-temperature metallic phase. It is suggested that the temperature T_G is the onset of an electronic Griffiths phase that has been theoretically proposed for Mott transitions with disorder. The experiment thus provides evidence of such a phase in an oxide system undergoing a Mott transition.

ACKNOWLEDGMENTS

The work has been supported by a sponsored project from the Science and Engineering Research Board (SERB), Government of India (Ref. No. EMR/2016/002855/PHY). A.K.R. thanks SERB for Distinguished Fellowship (Ref. No. SB/DF/008/2019). B.G. thanks the Science and Engineering Research Board (SERB), Govt. of India, Grant

No. EMR/2017/001990 for partial support. P.M. acknowledges Subhamita Sengupta for helpful suggestions related to

sample preparation. S.C. acknowledges Satyaki Kundu for his helpful suggestions.

-
- [1] D. Belitz and T. R. Kirkpatrick, *Rev. Mod. Phys.* **66**, 261 (1994).
- [2] K. Byczuk, W. Hofstetter, and D. Vollhardt, *Phys. Rev. Lett.* **94**, 056404 (2005).
- [3] T. Itou, E. Watanabe, S. Maegawa, A. Tajima, N. Tajima, K. Kubo, R. Kato, and K. Kanoda, *Sci. Adv.* **3**, e1601594 (2017).
- [4] A. E. Antipov, Y. Javanmard, P. Ribeiro, and S. Kirchner, *Phys. Rev. Lett.* **117**, 146601 (2016).
- [5] Y. G. Liang, S. Lee, H. S. Yu, H. R. Zhang, Y. J. Liang, P. Y. Zavalij, X. Chen, R. D. James, L. A. Bendersky, A. V. Davydov, and X. H. Zhang, *I. Takeuchi, Nat. Commun.* **11**, 3539 (2020).
- [6] V. Dobrosavljević and G. Kotliar, *Phys. Rev. Lett.* **78**, 3943 (1997).
- [7] M. C. O. Aguiar, V. Dobrosavljević, E. Abrahams, and G. Kotliar, *Phys. Rev. B* **71**, 205115 (2005).
- [8] E. C. Andrade, E. Miranda, and V. Dobrosavljević, *Phys. Rev. Lett.* **102**, 206403 (2009).
- [9] V. Dobrosavljević, N. Trivedi, and J. M. Valles, *Conductor-Insulator Quantum Phase Transitions* (Oxford University Press, Oxford, 2012).
- [10] D. Tanaskovic, E. Miranda, and V. Dobrosavljevic, *Phys. Rev. B* **70**, 205108 (2004).
- [11] T. Vojta, *AIP Conf. Proc.* **1550**, 188 (2013).
- [12] R. Yamamoto, T. Furukawa, K. Miyagawa, T. Sasaki, K. Kanoda, and T. Itou, *Phys. Rev. Lett.* **124**, 046404 (2020).
- [13] S. Middey, J. Chakhalian, P. Mahadevan, J. W. Freeland, A. J. Millis, and D. D. Sarma, *Annual. Rev. Mater. Res.* **46**, 305 (2016).
- [14] S. Catalano, M. Gibert, J. Fowlie, J. Íñiguez, J. M. Triscone and J. Kreise, *Rep. Prog. Phys.* **81**, 046501 (2018).
- [15] R. S. Bisht, S. Samanta, and A. K. Raychaudhuri, *Phys. Rev. B* **95**, 115147 (2017).
- [16] R. B. Griffiths, *Phys. Rev. Lett.* **23**, 17 (1969).
- [17] A. J. Hauser, E. Mikheev, N. E. Moreno, J. Hwang, J. Y. Zhang, and S. Stemmer, *Appl. Phys. Lett.* **106**, 092104 (2015).
- [18] J. H. Scofield, *Rev. Sci. Instr.* **58**, 985 (1987).
- [19] A. K. Raychaudhuri, *Curr. Opin. Solid State Mater. Sci.* **6**, 67 (2002).
- [20] A. Ghosh, S. Kar, A. Bid, and A. K. Raychaudhuri, [arXiv:condmat/0402130](https://arxiv.org/abs/condmat/0402130) v1.
- [21] S. Samanta, A. K. Raychaudhuri, X. Zhong, and A. Gupta, *Phys. Rev. B* **92**, 195125 (2015).
- [22] P. D. Welch, in *Modern Spectral Analysis*, edited by D. G. Childers, (IEEE Press, John Wiley and Sons, New York, 1978).
- [23] A. K. Raychaudhuri, *Adv. Phys.* **44**, 21 (1995).
- [24] R. S. Bisht, G. N. Daptary, A. Bid, and A. K. Raychaudhuri, *J. Phys.: Condens. Matter* **31**, 145603 (2019).
- [25] Jian Liu, M. Kareev, B. Gray, J. W. Kim, P. Ryan, B. Dabrowski, J. W. Freeland, and J. Chakhalian, *Appl. Phys. Lett.* **96**, 233110 (2010).
- [26] E. Mikheev, A. J. Hauser, B. Himmetoglu, N. E. Moreno, A. Janotti, C. G. Van de Walle, and S. Stemmer, *Sci. Adv.* **1**, e1500797 (2015).
- [27] See Supplemental Material at <http://link.aps.org/supplemental/10.1103/PhysRevMaterials.5.085005> for fitting of the DC resistivity, DC conductivity, and impedance spectroscopy data.
- [28] X. Granados, J. Fontcuberta, X. Obradors, and J. B. Torrance, *Phys. Rev. B* **46**, 15683 (1992).
- [29] D. Kumar, K. P. Rajeev, J. A. Alonso, and M. J. Martínez-Lope, *J. Phys.: Condens. Matter* **21**, 185402 (2009).
- [30] D. S. McLachlan, *J. Phys C: Solid State Phys.* **20**, 865 (1987).
- [31] A. Sahoo, S. D. Ha, S. Ramanathan, and A. Ghosh, *Phys. Rev. B* **90**, 085116 (2014).
- [32] A. M. Alsaqqa, S. Singh, S. Middey, M. Kareev, J. Chakhalian, and G. Sambandamurthy, *Phys. Rev. B* **95**, 125132 (2017).
- [33] G. N. Daptary, S. Kumar, M. Kareev, J. Chakhalian, A. Bid, and S. Middey, *Phys. Rev. B* **100**, 125105 (2019).
- [34] P. Dutta and P. M. Horn, *Rev. Mod. Phys.* **53**, 497 (1981).
- [35] Source of EIS: <http://www.abc.chemistry.bsu.by/vi/analyser/>.
- [36] P. Lunkenheimer and A. Loidl, *Phys. Rev. Lett.* **91**, 207601 (2003).
- [37] A. N. Papanthassasiou, I. Sakellis, and J. Grammatikakis, *Appl. Phys. Lett.* **91**, 122911 (2007).
- [38] J. Burgy, M. Mayr, V. Martin-Mayor, A. Moreo, and E. Dagotto, *Phys. Rev. Lett.* **87**, 277202 (2001).
- [39] M. B. Salamon, P. Lin, and S. H. Chun, *Phys. Rev. Lett.* **88**, 197203 (2002).
- [40] J. Deisenhofer, D. Braak, H.-A. Krug von Nidda, J. Hemberger, R. M. Eremina, V. A. Ivanshin, A. M. Balbashov, G. Jug, A. Loidl, T. Kimura, and Y. Tokura, *Phys. Rev. Lett.* **95**, 257202 (2005).
- [41] V. N. Krivoruchko, Y. Melikhov, and D. C. Jiles, *Phys. Rev. B* **77**, 180406(R) (2008).
- [42] R. D. Merithew, M. B. Weissman, F. M. Hess, P. Spradling, E. R. Nowak, J. O'Donnell, J. N. Eckstein, Y. Tokura, and Y. Tomioka, *Phys. Rev. Lett.* **84**, 3442 (2000).
- [43] R. H. Heffner, J. E. Sonier, D. E. MacLaughlin, G. J. Nieuwenhuys, G. Ehlers, F. Mezei, S.-W. Cheong, J. S. Gardner, and H. Röder, *Phys. Rev. Lett.* **85**, 3285 (2000).
- [44] V. N. Krivoruchko, M. A. Marchenko, and Y. Melikhov, *Phys. Rev. B* **82**, 064419 (2010).